

Fabrication of hierarchical photonic nanostructures inspired by *Morpho* butterflies utilizing laser interference lithography

Radwanul Hasan Siddique,^{1,*} Ruben Hünig,² Abrar Faisal,¹ Uli Lemmer,^{1,2} and Hendrik Hölscher¹

¹*Institute for Microstructure Technology (IMT), Karlsruhe Institute of Technology (KIT), Hermann-von-Helmholtz-Platz 1, 76344 Eggenstein-Leopoldshafen, Germany*

²*Light Technology Institute (LTI), Karlsruhe Institute of Technology (KIT), 76131 Karlsruhe, Germany*

[*radwanul.siddique@kit.edu](mailto:radwanul.siddique@kit.edu)

Abstract: We introduce laser interference lithography (LIL) as a tool to fabricate hierarchical photonic nanostructures inspired by blue *Morpho* butterflies. For that, we utilize the interference pattern in vertical direction in addition to the conventional horizontal one. The vertical interference creates the lamellae by exploiting the back reflection from the substrate. The horizontal interference patterns the ridges of the hierarchical Christmas tree like structure. The artificial *Morpho* replica produced with this technique feature a brilliant blue iridescence up to an incident angle of 40°.

© 2015 Optical Society of America

OCIS codes: (260.2110) Electromagnetic optics; (220.3740) Lithography; (220.4241) Nanos-structure fabrication; (310.6628) Subwavelength structures, nanostructures; (050.0050) Diffraction and gratings; (330.0330) Vision, color, and visual optics; (000.1430) Biology and medicine; (350.4238) Nanophotonics and photonic crystals.

References and links

1. W. W. Ng, C.-S. Hong, and A. Yariv, "Holographic interference lithography for integrated optics," *IEEE Trans. Elect. Dev.* **25**(10), 1193-1200 (1978).
2. N. N. Efremow, "A simple technique for modifying the profile of resist exposed by holographic lithography," *J. Vac. Sci. Tech.* **19**(4), 1234-1237 (1981).
3. A. Fernandez, J. Decker, S. Herman, D. Phillion, D. Sweeney, and M. Perry, "Methods for fabricating arrays of holes using interference lithography," *J. Vac. Sci. Tech. B* **15**(6), 2439-2443 (1997).
4. M. Campbell, D. Sharp, M. Harrison, R. Denning, and A. Turberfield, "Fabrication of photonic crystals for the visible spectrum by holographic lithography," *Nature* **404**(6773), 53-56 (2000).
5. S. Brueck, "Optical and interferometric lithography-Nanotechnology enablers," *Proc. IEEE* **93**(10), 1704-1721 (2005).
6. J.-H. Jang, C. Ullal, M. Maldovan, T. Gorishnyy, S. Kooi, C. Koh, and E. Thomas, "3D micro- and nanostructures via interference lithography," *Adv. Funct. Mater.* **17**(16), 3027-3041 (2007).
7. M. Maldovan and E. L. Thomas, *Periodic materials and interference lithography: for photonics, phononics and mechanics* (John Wiley & Sons, 2009).
8. C. Lu and R. H. Lipson, "Interference lithography: a powerful tool for fabricating periodic structures," *Laser Photon. Rev.* **4**(4), 568-580 (2010).
9. H. van Wolferen and L. Abelman, in *Lithography: principles, processes and materials*, edited by T. C. Hennessy (Nova Publishers, Hauppauge NY, USA, 2011) pp. 133-148, open Access.
10. K. S. Cho, P. Mandal, K. Kim, I. H. Baek, S. Lee, H. Lim, D. J. Cho, S. Kim, J. Lee, and F. Rotermund, "Improved efficiency in GaAs solar cells by 1D and 2D nanopatterns fabricated by laser interference lithography," *Opt. Commun.* **284**(10), 2608-2612 (2011).

11. S. H. Kim, K.-D. Lee, J.-Y. Kim, M.-K. Kwon, and S.-J. Park, "Fabrication of photonic crystal structures on light emitting diodes by nanoimprint lithography," *Nanotech.* **18**(5), 055306 (2007).
12. H.-J. Eisler, V. C. Sundar, M. G. Bawendi, M. Walsh, H. I. Smith, and V. Klimov, "Color-selective semiconductor nanocrystal laser," *Appl. Phys. Lett.* **80**(24), 4614-4616(2002).
13. M. Farhoud, J. Ferrera, A. J. Lochtefeld, T. E. Murphy, M. L. Schattenburg, J. Carter, C. A. Ross, and H. I. Smith, "Fabrication of 200 nm period nanomagnet arrays using interference lithography and a negative resist," *J. Vac. Sci. Tech. B* **17**(6), 3182-3185 (1999).
14. F. Yu, F. Mcklich, P. Li, H. Shen, S. Mathur, C.-M. Lehr, and U. Bakowsky, "In vitro cell response to a polymer surface micropatterned by laser interference lithography," *Biomacromol.* **6**(3), 1160-1167 (2005).
15. J. H. Moon, J. Ford, and S. Yang, "Fabricating three-dimensional polymeric photonic structures by multi-beam interference lithography," *Polym. Adv. Tech.* **17**(2), 83-93 (2006).
16. J. Schilling, F. Miller, S. Matthias, R. B. Wehrspohn, U. Gsele, and K. Busch, "Three-dimensional photonic crystals based on macroporous silicon with modulated pore diameter," *Appl. Phys. Lett.* **78**(9), 1180-1182 (2001).
17. S.-Y. Lin, E. Chow, V. Hietala, P. R. Villeneuve, and J. D. Joannopoulos, "Experimental demonstration of guiding and bending of electromagnetic waves in a photonic crystal," *Science* **282**(5387), 274-276 (1998).
18. S. Noda, A. Chutinan, and M. Imada, "Trapping and emission of photons by a single defect in a photonic bandgap structure," *Nature* **407**(6804), 608-610 (2000).
19. A. Talneau, L. Le Gouezigou, N. Bouadma, M. Kafesaki, C. M. Soukoulis, and M. Agio, "Photonic-crystal ultrashort bends with improved transmission and low reflection at 1.55 μm ," *Appl. Phys. Lett.* **80**(4), 547-549 (2002).
20. B. Bläsi, H. Hauser, O. Höhn, V. Kübler, M. Peters, and A. J. Wolf, "Photon management structures originated by interference lithography," *Energy Proc.* **8**, 712-718 (2011).
21. E. Yablonovitch, "Inhibited spontaneous emission in solid-state physics and electronics," *Phys. Rev. Lett.* **58**(20), 2059 (1987).
22. S. John, "Strong localization of photons in certain disordered dielectric superlattices," *Phys. Rev. Lett.* **58**(23), 2486 (1987).
23. A. R. Parker, "515 million years of structural colour," *J. Opt. A Pure Appl. Opt.* **2**(6), R15-R28 (2000).
24. P. Vukusic and J. R. Sambles, "Photonic structures in biology," *Nature* **424**(6950), 852-855 (2003).
25. T. Starkey and P. Vukusic, "Light manipulation principles in biological photonic systems," *Nanophoton.* **2**(4), 289-307 (2013).
26. L. Dellieu, M. Sarrazin, P. Simonis, O. Deparis, and J. P. Vigneron, "A two-in-one superhydrophobic and anti-reflective nanodevice in the grey cicada *Cicada orni* (Hemiptera)," *J. Appl. Phys.* **116**(2), 024701 (2014).
27. P. Vukusic, J. R. Sambles, C. R. Lawrence, and R. J. Wootton, "Quantified interference and diffraction in single Morpho butterfly scales," *Proc. R. Soc. B Biol. Sci.* **266**(1427), 1403-1411 (1999).
28. S. Kinoshita, S. Yoshioka, and K. Kawagoe, "Mechanisms of structural colour in the Morpho butterfly: cooperation of regularity and irregularity in an iridescent scale," *Proc. R. Soc. B Biol. Sci.* **269**(1499), 1417-1421 (2002).
29. R. H. Siddique, S. Diewald, J. Leuthold, and H. Hölscher, "Theoretical and experimental analysis of the structural pattern responsible for the iridescence of Morpho butterflies," *Opt. Express* **21**(12), 14351-14361 (2013).
30. Y. Zheng, X. Gao, and L. Jiang, "Directional adhesion of superhydrophobic butterfly wings," *Soft Mat.* **3**(2), 178-182 (2007).
31. R. A. Potyrailo, H. Ghiradella, A. Vertiatchikh, K. Dovidenko, J. R. Cournoyer, and E. Olson, "Morpho butterfly wing scales demonstrate highly selective vapour response," *Nat. Photon.* **1**(2), 123-128 (2007).
32. A. D. Pris, Y. Utturkar, C. Surman, W. G. Morris, A. Vert, S. Zalyubovskiy, T. Deng, H. T. Ghiradella, and R. A. Potyrailo, "Towards high-speed imaging of infrared photons with bio-inspired nanoarchitectures," *Nat. Photon.* **6**(3), 195-200 (2012).
33. F. Zhang, Q. Shen, X. Shi, S. Li, W. Wang, Z. Luo, G. He, P. Zhang, P. Tao, C. Song, W. Zhang, D. Zhang, T. Deng, and W. Shang, "Infrared detection based on localized modification of Morpho butterfly wings," *Adv. Mat.* **27**, 10771082 (2015).
34. S. Lou, X. Guo, T. Fan, and D. Zhang, "Butterflies: inspiration for solar cells and sunlight water-splitting catalysts," *Energy Env. Sci.* **5**(11), 9195-9216 (2012).
35. MicroChemicals GmbH®, "Az@ 1500-series," .
36. W. Menz, J. Mohr, and O. Paul, "Lithography," in *Microsystem Technology* (Wiley-VCH Verlag GmbH, 2007) pp. 171-208.
37. T. Bocksrocker, *Technologien für das Lichtmanagement in organischen Leuchtdioden*, PhD thesis, Zugl.: Karlsruhe, Karlsruher Institut für Technologie (KIT), Diss., 2013.
38. R. H. Siddique, A. Faisal, R. Hünig, C. Bartels, I. Wacker, U. Lemmer, and H. Hölscher, "Utilizing laser interference lithography to fabricate hierarchical optical active nanostructures inspired by the blue Morpho butterfly," *Proc. SPIE* **9187**, The Nature of Light: Light in Nature V, 91870E-91870E (2014).
39. H. A. Macleod, *Thin-film optical filters* (IOP Publishing Ltd, 1986).
40. M. Kolle, P. M. Salgard-Cunha, M. R. J. Scherer, F. Huang, P. Vukusic, S. Mahajan, J. J. Baumberg, and U. Steiner, "Mimicking the colourful wing scale structure of the *Papilio blumei* butterfly," *Nat. Nanotech.* **5**(7),

- 511-515 (2010).
41. A. Saito, J. Murase, M. Yonezawa, H. Watanabe, T. Shibuya, M. Sasaki, T. Ninomiya, S. Noguchi, M. Akai-kasaya, and Y. Kuwahara, "High-throughput reproduction of the *Morpho* butterfly's specific high contrast blue," Proc. SPIE **8339**, 83390C-83390C (2012).
 42. K. Chung, S. Yu, C.-J. Heo, J. W. Shim, S.-M. Yang, M. G. Han, H.-S. Lee, Y. Jin, S. Y. Lee, N. Park, and J. H. Shin, "Flexible, angle-independent, structural color reflectors inspired by *Morpho* butterfly wings," Adv. Mat. **24**(18), 2375-2379 (2012).
 43. K. Chung and J. H. Shin, "Range and stability of structural colors generated by *Morpho*-inspired color reflectors," J. Opt. Soc. Am. A **30**(5), 962-968 (2013).
 44. S. Yoshioka and S. Kinoshita, "Polarization-sensitive color mixing in the wing of the Madagascan sunset moth," Opt. express **15**(5), 2691-2701 (2007).
 45. S. Yoshioka, T. Nakano, Y. Nozue, and S. Kinoshita, "Coloration using higher order optical interference in the wing pattern of the Madagascan sunset moth," J. R. Soc. Int. **5**(21), 457-464 (2008).
 46. P. Vukusic, J. R. Sambles, and C. R. Lawrence, "Colour mixing in wing scales of a butterfly," Nature **404**(6777), 457-457 (2000).
 47. A. E. Seago, P. Brady, J.-P. Vigneron, and T. D. Schultz, "Gold bugs and beyond: a review of iridescence and structural colour mechanisms in beetles (Coleoptera)," J. R. Soc. Int. **6**((Suppl 2)), S165-S184 (2009).
 48. S. Vignolini, E. Moyroud, B. J. Glover, and U. Steiner, "Analysing photonic structures in plants," J. R. Soc. Int. **10**(87), 20130394 (2013).
-

1. Introduction

Laser interference lithography (LIL) is used for decades to pattern surfaces with periodic structures ranging from micron to sub-micron scales [1–9]. This technique allows to write 1D, 2D, and even 3-dimensional periodic patterns into a photoresist by adjusting the intensity, geometry, polarization, and phase of the applied laser light [6–8]. Since the fabrication of nano- and microstructured surfaces is a parallel process, LIL is competitive to other high-resolution lithographic techniques. Consequently, it is used for various industrial applications including but not limited to the field of solar cells and LED [10, 11], laser technology [12], integrated optical design [1], data storage [13], optical communications [5], biomedical applications [14] and IC industries [8].

A very interesting application of LIL is the manufacturing of photonic crystals (PC) [6, 8, 15] and it has been implemented for applications like filters [16], waveguides [17], resonant cavities [18], PC-based optical elements [19] and light management in thin film solar cells [20]. The concept of photonic crystal was born in the late 1980s [21, 22]. In nature, however, there are many examples of 1D, 2D, and 3D photonic crystals found in plants and insects which evolved several million years ago [23–25]. Frequently, these nano- and microstructures are multifunctional [26]. Evolutionary optimized scales of the famous *Morpho* butterfly, for example, give at the same time a strong blue coloration [27–29] and make the wing hydrophobic [30]. It has been demonstrated that by mimicking such structures it is possible to outperform existing photonic vapor sensors [31] and thermal sensors [32, 33] in sensitivity and spatial resolution. Furthermore, butterflies inspired the development of nanostructures enhancing the efficiency of solar cells and water-splitting [34].

Here, we introduce a technique to fabricate the hierarchical 'Christmas tree' like morphology of *Morpho* butterflies utilizing dual beam laser interference lithography. In difference to the conventional approach, where vertical reflection is suppressed by anti-reflective coatings, we specifically use a reflective coating below the resist to create an additional vertical interference along with the horizontal one. In this way, the vertical standing wave pattern creates the lamellae while the horizontal interference structures pattern ridges. A low contrast photoresist is used to obtain the triangular tapered shape. Depending on the period of the vertical standing wave and the photoresist material, the thickness of the lamellae and the gap between them can be controlled. These parameters directly influence the structural color of the final photonic structure. The artificially replicated *Morpho* structure produced in this way shows brilliant blue

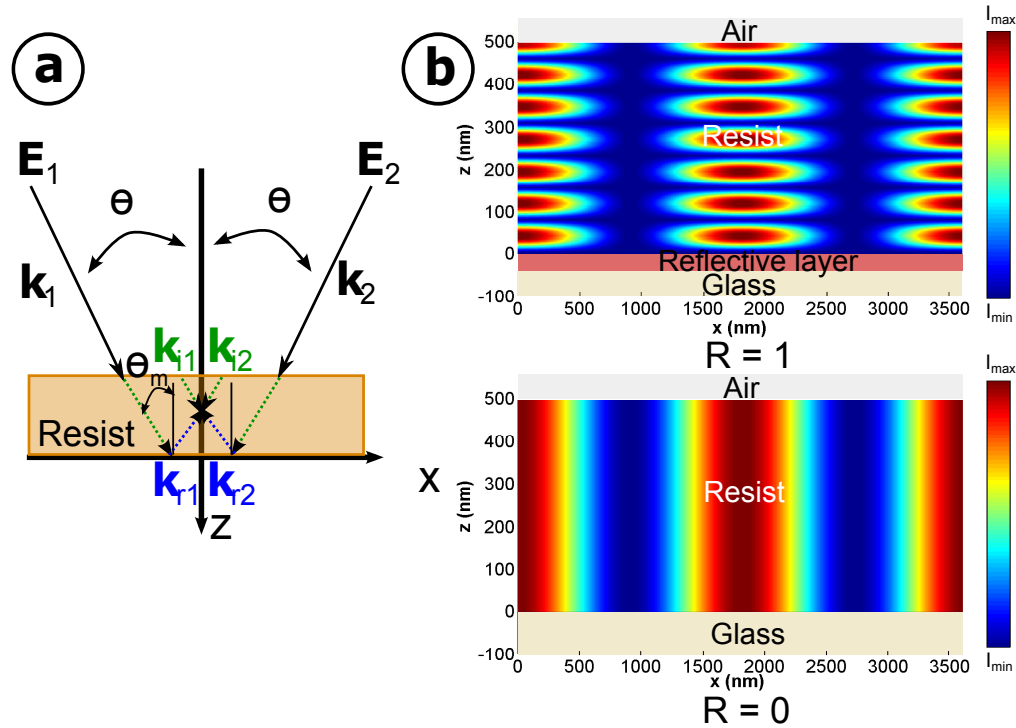


Fig. 1. (a) Schematic of the wave vectors for a dual beam interference. (b) The calculated dual beam standing wave patterns in the 500 nm thick resist with and without back reflection from the substrate. If the reflection factor R is close to 1, the vertical standing waves create multilayer stacks of air and polymer. The vertical standing waves, however, disappear if the back reflection intensity is 0 ($R = 0$).

iridescence up to an incident angle of 40° .

2. Theoretical background

In general, the interference of two beams of coherent light results in horizontal periodic patterns consisting of dark and bright areas. In laser interference lithography (LIL) this pattern is transferred into a photoresist to obtain nano- and microstructures. The conventional theory of dual beam laser interference lithography assumes the superposition of two incoming electromagnetic plane waves with the same angular frequency ω propagating simultaneously in the same medium [7–9]. A schematic considering also the beams reflected from the substrate is shown in Fig. 1(a).

The superimposed incident electric field will be the sum of the electric fields of the individual plane waves at any given point in space

$$\mathbf{E}_h(\mathbf{r}, t) = \mathbf{E}_1 e^{i(\mathbf{k}_1 \cdot \mathbf{r} - \omega t)} + \mathbf{E}_2 e^{i(\mathbf{k}_2 \cdot \mathbf{r} - \omega t)} \quad (1)$$

where \mathbf{E}_1 and \mathbf{E}_2 are the complex electric field amplitude vectors of the incident beams and \mathbf{k}_1 and \mathbf{k}_2 are the corresponding wave vectors. If the waves propagate with an angle $\pm\theta$ to the normal shown in the Fig. 1(a) and $\Delta\varphi$ is the relative phase difference between the two waves,

the electric field amplitude vectors and wave vectors are given by

$$\mathbf{E}_1 = E_0 \hat{\mathbf{n}}, \mathbf{k}_1 = \frac{2\pi n}{\lambda} (\sin \theta, 0, \cos \theta) \quad (2)$$

$$\mathbf{E}_2 = E_0 e^{i\Delta\varphi} \hat{\mathbf{n}}, \mathbf{k}_2 = \frac{2\pi n}{\lambda} (-\sin \theta, 0, \cos \theta) \quad (3)$$

Here, E_0 is the amplitude of the incoming electric fields, λ is the wavelength of the exposure beam, and n is the refractive index of the medium (1 for air in this case). $\hat{\mathbf{n}}$ defines the polarization of the electric fields. As the spatial interference distributes along x-axis we calculate the resulting horizontal interference in the x-plane, i.e., $\mathbf{r} = (x, 0, 0)$ and inserting all parameters together with Eqs. (2) and (3), we obtain the spatial distribution of the horizontal interference for a given polarization [7]

$$\begin{aligned} I_h(\mathbf{r}) &= |\mathbf{E}_h(\mathbf{r})|^2 = \mathbf{E}_h(\mathbf{r}) \cdot \mathbf{E}_h^*(\mathbf{r}) \\ &= 2I_0 \left(1 + \cos\left(\frac{4\pi}{\lambda} \sin \theta x - \Delta\varphi\right) \right) \end{aligned} \quad (4)$$

where, I_0 is the intensity of the incident beams and equals to $|E_0|^2$. We can easily calculate the horizontal period of the interference pattern from the modulation cosine term in Eq. (4). The phase difference $\Delta\varphi$ between the complex amplitudes only translates the interference pattern in space without changing its shape. The intensity maxima will be achieved at every multiple of 2π , i.e., spatially in every multiple of $\frac{\lambda}{2\sin\theta}$. Hence, the period of the horizontal grating is given by

$$P_h = \frac{\lambda}{2\sin\theta} \quad (5)$$

If we consider now a possible back reflection from the substrate, the resultant of the exposure beams and back reflected beams will create an additional interference vertically in the resist and the spatial standing wave pattern distributes in the x – z plane, i.e., $\mathbf{r} = (x, 0, z)$.

$$\mathbf{E}_v(\mathbf{r}, t) = \mathbf{E}_{i1} e^{i(\mathbf{k}_{i1} \cdot \mathbf{r} - \omega t)} + \mathbf{E}_{i2} e^{i(\mathbf{k}_{i2} \cdot \mathbf{r} - \omega t)} + \mathbf{E}_{r1} e^{i(\mathbf{k}_{r1} \cdot \mathbf{r} - \omega t)} + \mathbf{E}_{r2} e^{i(\mathbf{k}_{r2} \cdot \mathbf{r} - \omega t)} \quad (6)$$

Here, all four incident (\mathbf{E}_{i1} and \mathbf{E}_{i2}) and reflected (\mathbf{E}_{r1} and \mathbf{E}_{r2}) electric field amplitude vectors and corresponding wave vectors (\mathbf{k}_{i1} , \mathbf{k}_{i2} , \mathbf{k}_{r1} , and \mathbf{k}_{r2}) can be described by

$$\mathbf{E}_{i1} = E_0 \hat{\mathbf{n}}, \mathbf{k}_{i1} = \frac{2\pi n_m}{\lambda} (\sin \theta_m, 0, \cos \theta_m) \quad (7)$$

$$\mathbf{E}_{i2} = E_0 e^{i(\Delta\varphi)} \hat{\mathbf{n}}, \mathbf{k}_{i2} = \frac{2\pi n_m}{\lambda} (-\sin \theta_m, 0, \cos \theta_m) \quad (8)$$

$$\mathbf{E}_{r1} = rE_0 e^{i\pi} \hat{\mathbf{n}}, \mathbf{k}_{r1} = \frac{2\pi n_m}{\lambda} (\sin \theta_m, 0, -\cos \theta_m) \quad (9)$$

$$\mathbf{E}_{r2} = rE_0 e^{i(\Delta\varphi - \pi)} \hat{\mathbf{n}}, \mathbf{k}_{r2} = \frac{2\pi n_m}{\lambda} (-\sin \theta_m, 0, -\cos \theta_m) \quad (10)$$

where, r is the fraction of the incident electric fields which reflects back and θ_m is the refracted angle in the photoresist. As the interference occurs within the resist, the refractive index n_m of the material is considered for the wave vectors. Furthermore, there is a phase shift of π in the reflected electric fields with respect to incident beams. Similarly, we can calculate the

vertical interference of the incoming incident and the back-reflected beams as previously and the vertical standing wave intensity distribution is given by

$$\begin{aligned}
I_v(\mathbf{r}) &= |\mathbf{E}_v(\mathbf{r})|^2 = \mathbf{E}_v(\mathbf{r}) \cdot \mathbf{E}_v^*(\mathbf{r}) \\
&= 2(1+R)|\mathbf{E}_0|^2 + \\
&2\text{Re}(\mathbf{E}_{i1} \cdot \mathbf{E}_{i2}^*) \cos[(\mathbf{k}_{i1} - \mathbf{k}_{i2}) \cdot \mathbf{r}] - 2\text{Im}(\mathbf{E}_{i1} \cdot \mathbf{E}_{i2}^*) \sin[(\mathbf{k}_{i1} - \mathbf{k}_{i2}) \cdot \mathbf{r}] + \\
&2\text{Re}(\mathbf{E}_{i1} \cdot \mathbf{E}_{r1}^*) \cos[(\mathbf{k}_{i1} - \mathbf{k}_{r1}) \cdot \mathbf{r}] - 2\text{Im}(\mathbf{E}_{i1} \cdot \mathbf{E}_{r1}^*) \sin[(\mathbf{k}_{i1} - \mathbf{k}_{r1}) \cdot \mathbf{r}] + \\
&2\text{Re}(\mathbf{E}_{i1} \cdot \mathbf{E}_{r2}^*) \cos[(\mathbf{k}_{i1} - \mathbf{k}_{r2}) \cdot \mathbf{r}] - 2\text{Im}(\mathbf{E}_{i1} \cdot \mathbf{E}_{r2}^*) \sin[(\mathbf{k}_{i1} - \mathbf{k}_{r2}) \cdot \mathbf{r}] + \\
&2\text{Re}(\mathbf{E}_{i2} \cdot \mathbf{E}_{r2}^*) \cos[(\mathbf{k}_{i2} - \mathbf{k}_{r2}) \cdot \mathbf{r}] - 2\text{Im}(\mathbf{E}_{i2} \cdot \mathbf{E}_{r2}^*) \sin[(\mathbf{k}_{i2} - \mathbf{k}_{r2}) \cdot \mathbf{r}] + \\
&2\text{Re}(\mathbf{E}_{i2} \cdot \mathbf{E}_{r1}^*) \cos[(\mathbf{k}_{i2} - \mathbf{k}_{r1}) \cdot \mathbf{r}] - 2\text{Im}(\mathbf{E}_{i2} \cdot \mathbf{E}_{r1}^*) \sin[(\mathbf{k}_{i2} - \mathbf{k}_{r1}) \cdot \mathbf{r}] + \\
&2\text{Re}(\mathbf{E}_{r1} \cdot \mathbf{E}_{r2}^*) \cos[(\mathbf{k}_{r1} - \mathbf{k}_{r2}) \cdot \mathbf{r}] - 2\text{Im}(\mathbf{E}_{r1} \cdot \mathbf{E}_{r2}^*) \sin[(\mathbf{k}_{r1} - \mathbf{k}_{r2}) \cdot \mathbf{r}] \\
&= 2I_0 \left[\left(1 + R - 2\sqrt{R} \cos\left(\frac{4\pi n_m}{\lambda} \cos \theta_m z\right) \right) \left(1 + \cos\left(\frac{4\pi n_m}{\lambda} \sin \theta_m x - \Delta\phi\right) \right) \right]
\end{aligned} \tag{11}$$

Here, R is the reflection co-efficient which equals to r^2 . The vertical standing wave period is therefore $\frac{\lambda}{2n_m \cos \theta_m}$. We can calculate θ_m using the Snell's law and thus the vertical grating period is given by

$$P_v = \frac{\lambda}{2n_m \cos(\sin^{-1}(\sin \theta / n_m))} \tag{12}$$

Assuming that the horizontal and vertical standing waves superimpose, the final distribution pattern can be calculated from

$$\begin{aligned}
I(\mathbf{r}) &= 2I_0 \left[1 + \cos\left(\frac{4\pi}{\lambda} \sin \theta x - \Delta\phi\right) + \right. \\
&\left. \left(1 + R - 2\sqrt{R} \cos\left(\frac{4\pi n_m}{\lambda} \cos \theta_m z\right) \right) \left(1 + \cos\left(\frac{4\pi n_m}{\lambda} \sin \theta_m x - \Delta\phi\right) \right) \right]
\end{aligned} \tag{13}$$

We calculated the spatial intensity distribution of the resulting standing wave pattern with this equation considering a 500 nm thick AZ resist material ($n_m = 1.71$) [35] for an incident beam of 266 nm with an angle of $\theta = 4.2$. The result is shown in Fig. 1(b) with ($R = 1$) and without ($R = 0$) back-reflection from the substrate. The horizontal and vertical intensities peak to peak distance are approximately 1.8 μm and 78 nm, respectively. Six intensity knots are visible in the 500 nm thick resist resulting in six 'lamellae' with a thickness of 40 nm. As already discussed, the vertical interference disappears completely if the substrate yields no back-reflection.

3. Fabrication process

Based on the above-described theory we fabricated Morpho inspired structures by laser interference lithography. The fabrication process mainly includes three steps: sample preparation, exposure and development. They are compared in Fig. 2(a) for conventional LIL and for the presented approach. The important difference is the evaporation of the reflective layer on the substrate. For our specific application of hierarchical Morpho structures, the reflective layer has to be reflective at the exposure wavelength but mostly transparent in the visible range. An aluminium substrate might be chosen for deep UV exposure as it reflects more than 90 % of the incoming beam at the exposure wavelength of 266 nm. However, in order to improve the optical properties in visible wavelength regime, we used fused silica (25 mm \times 25 mm \times 1 mm) as a substrate and sputtered with a thin reflective optical coating which has a reflectivity of 99.5 % at wavelengths of 250-280 nm by LASEROPTIK GmbH, Garbsen, Germany. The average reflectance of the coating is well below than 5 % in the visible range. A positive photoresist (AZ 1505, Microchemicals GmbH, Ulm, Germany) is spun on the substrate with a speed

of 3000 rpm, an acceleration of 1500 rpm/s for 60 seconds to achieve 500 nm thickness. The prebake was performed on a hotplate at 95°C for 3 minutes. The parameters were chosen adequately to realize a low contrast system, allowing for direct transfer of the interference pattern into the photoresist [36].

It is worth mentioning that in conventional LIL an anti-reflective coating is frequently evaporated onto the sample to avoid back reflection from the silicon or reflective metallic substrate and prevent any vertical patterning [9]. To demonstrate the difference between these two approaches we also prepared samples without reflective coating, i.e., we spun the same resist directly on the silica substrates.

We exposed these two types of samples using the experimental set-up sketched in Fig. 2(b). It is a two-beam LIL in a Mach-Zehnder configuration [37, 38]. In order to satisfy the high coherence requirement of LIL, two incident laser beams have been split from the same laser source, and hold same-scale optical paths when reaching to the exposure surface. We chose AZ photoresist which has low sensitivity for the exposure wavelength (266 nm) so that we can get triangular or tapered shape like structure as of 'Christmas tree' nanostructures of *Morpho* butterfly. The KOH-based AZ 400K (1 : 4 diluted) developer (Microchemicals GmbH, Ulm, Germany) is used to develop the sample for 15 seconds to achieve the proper triangular shape with an exposure dosage of 250 mJ/cm² [36].

The SEM image of the finally obtained structure is displayed in Fig. 2(c). Due to the optimization of exposure dosage of low-contrast resist and development parameters, the horizontal grating has a triangular shape and resembles the ridges. The vertical structure caused by the back reflection from the reflective coating on the other hand mimics the lamellae. The multilayer of air/polymer is clearly visible and the corresponding blue appearance is included in the Fig. 3. The structural color is mainly due to the hierarchical pattern which can be easily noticed in comparison with only triangular structure. The detailed optical properties will be analyzed in the following section. The horizontal period of the structures in x-y plane is around $1.8 \pm 0.1 \mu\text{m}$ which can be affirmed by Eq. (5) for an exposure incident angle (θ) of 4.2°. The vertical period can also be calculated via Eq. (12). The approximated refractive index of the material is 1.71 at a wavelength of 266 nm [35] and therefore, the vertical period is calculated to be 77.9 nm. The experimental value of the vertical period is found to be $80 \pm 3 \text{ nm}$ which fits nicely to the theoretical result.

4. Optical characterization and discussion

Due to the *Morpho*-type structure the final sample has a blue color and the different optical appearance of the two sample types can be seen with the naked eye. As shown in Fig. 3 the *Morpho*-type sample appears blue even for large view angles of 40° while the triangular structure without vertical lamellae ($R = 0$) exhibits regular grating effect at high angles.

The quantitative optical characterization of the fabricated structures analyzed with a UV-Vis spectrometer is shown in Fig. 4. As depicted in Fig. 4(a), the triangular shaped *Morpho*-type structure has a reflection of around 30 % for wavelengths between 380 nm and 460 nm at normal incidence while only negligible reflection of about 2 % is observed for the triangular grating. Consequently, it is evident that the blue reflectance is due to the 5 layers of air and polymer. The thickness of each of the polymer layers is approximately 40 nm and the air gap within the layers is also about 40 nm. The achieved thickness of the layers, however, produce only a secondary reflection peak in the visible regime. We calculated the high order reflection peak wavelengths at normal incidence with the transfer matrix method [39] for a five-fold stack of air and polymer layers and found two maxima at 410 nm and 605 nm in the visible regime (dashed line in Fig. 4(a)). These peak positions coincide with the experimental spectrum. The overall reflection intensity of the *Morpho*-type sample, however, is higher than the theoretical values

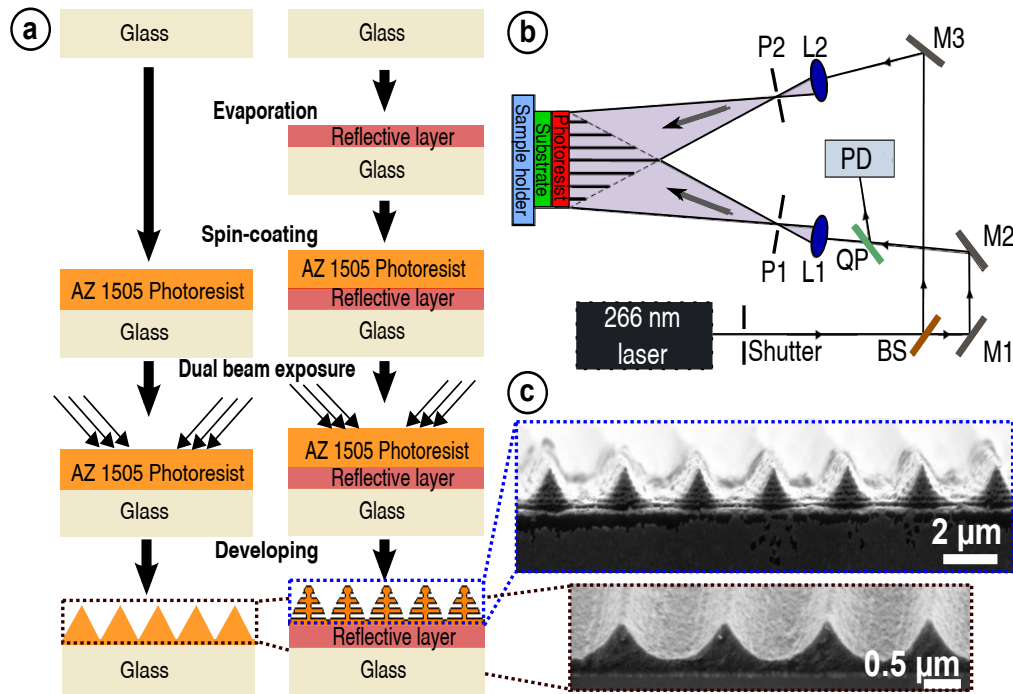


Fig. 2. (a) Flow diagram of the fabrication process of hierarchical optical structures in *Morpho* butterfly scale using dual beam laser interference lithography and compare it to a regular dual beam LIL process. (b) The schematic of the lithography setup: BS – Beam Splitter, M – Mirror, QP – Quartz Plate, L – Lens, PD – Photodetector, P – Pinhole. (c) The cross-sectional view of the fabricated *Morpho* sample ($R = 1$) shows the tapered shaped polymer/air multilayers. The other considered fabricated sample of triangular grating ($R = 0$) is shown below for comparison.

but lower than first order peaks. This might be an effect of 'non-ideal' behavior (uneven optical thicknesses of two layers) of the multilayer or due to the experimental irregularities of the structure [44, 45]. We were only able to structure high order interference peaks due to the given exposure wavelength. The thickness of the layer depends on the exposure wavelength (Eq. (12)). The bandwidth of the reflected blue $\Delta\lambda$ is about 125 nm. This value is close to the theoretical value of $\Delta\lambda_{th} = (2/\pi)\bar{\lambda}(\Delta n/\bar{n}) = 132$ nm [40] where $\bar{\lambda}$ is the peak-center wavelength (424 nm), $\Delta n = 0.65$ the refractive index difference, and \bar{n} the averaged refractive index of the air and resist (1.325).

Calculating the bandwidth for the original *Morpho* butterfly with a refractive index of 1.56 [27] gives a value of 118 nm which is close to our experimental value. For the same reflection peak other fabricated *Morpho* inspired multilayer replicas [41, 42] made from TiO_2 ($n \approx 2.6$) and SiO_2 ($n \approx 1.5$) had a higher bandwidth of 145 nm. As a lower $\Delta n/\bar{n}$, i.e., bandwidth is important for a larger color gamut and better color stability of the structural colors [43] our fabrication technique exhibits competitive optical properties.

The fascinating phenomena of the *Morpho* nanostructures is their quasi-omnidirectional blue non-iridescent reflection [27–29]. If we use the classical equation for thin film interference $m\frac{\lambda}{2} = d_1(n_1 - \sin^2\theta)^{1/2} + d_2(n_2 - \sin^2\theta)^{1/2}$ (see, e.g., Eq. (1) in [40]) the peak reflection wavelength shifts approximately by 35 nm for an incident angle of 30° . This effect, however, is not observed for *Morpho* butterflies [27, 28] as well as for our *Morpho* inspired structures. The

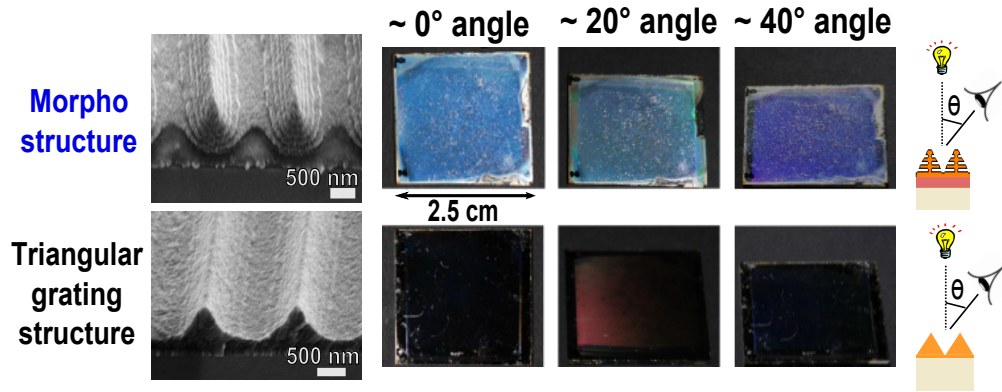


Fig. 3. The optical appearance of the fabricated sample exhibits a bright blue iridescence as *Morpho* butterfly wing till 40° of incident angle. The replicated structure is compared to normal triangular grating structures to demonstrate the difference in optical property. The SEM images of both structures are shown for comparison.

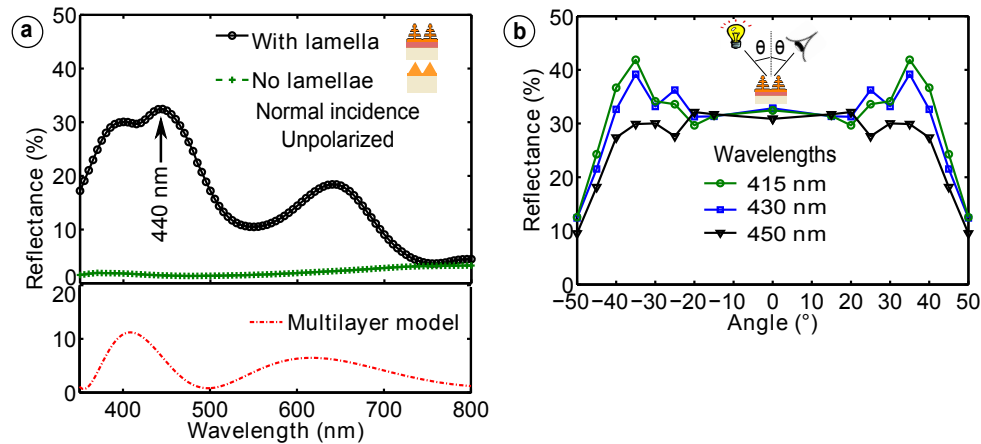


Fig. 4. (a) The reflection spectra of the fabricated samples show a reflection of 30% in the blue regime for normal incidence. The peak reflection of 33% is observed at a wavelength of 440 nm. The reflection is only about 2% for the triangular grating without lamellae for the same wavelength. The theoretical reflectance spectrum for a five-fold stack of air and resist with similar refractive indices is shown below. The positions of the reflection peaks correspond to the experimental ones. (b) The angle resolved reflection spectra reveals the high reflection of blue light for angles up to 40° for wavelengths of 415 nm, 430 nm and 450 nm. The reflection increases to 42% at an angle of 35° for the wavelength of 415 nm.

reflection peak stays in blue regime till an angle of 40° (see Fig. 4(b)). It is mainly due to the tapered shape of the multilayer air-polymer structures [29]. The tapered or so called 'Christmas tree' shape creates an impedance matching to the blue wavelength for higher incident angle. A rise of the reflection can be observed for an angle of 30° because of the guided mode resonance of the horizontal diffraction ridge/grating pattern.

5. Conclusion and outlook

To conclude, we demonstrated the advantage of laser interference lithography for the large scale fabrication of *Morpho* butterfly inspired 'Christmas tree' like hierarchical structures. We exploit the common issue of back reflection from the substrate and specifically used it to create the vertical interference to create the lamella pattern of the *Morpho* butterfly. Our fabricated *Morpho* replica mimic the most important feature of the original scales, namely the non-iridescent blue reflection for large angles in addition to the hydrophobic property [38]. Our proposed fabrication technique could be implemented to manufacture the multi-functional structures found in other insects and plants that feature structural colors caused by multilayer stacks of air and biopolymers [46–48].

The presented technique can be even improved. First of all, higher exposure wavelengths in UV-blue regime will give larger vertical interference period and thus high intense first order reflection in the visible regime. An increase of the number of layers will increase the reflection intensity and the aspect ratio of the ridges at the same time. By increasing the height of the structures, the hydrophobicity of the surface will be improved too and might turn the surface into a superhydrophobic optical coating. As photoresists have lower sensitivity in the current exposure wavelength, it requires already higher exposure time and dosage to expose a 500 nm thick resist. The low sensitivity of the resist is necessary to obtain the tapered shape of the 'Christmas tree' like shape for quasi-omnidirectional blue reflection. Therefore, a trade off between achieving non-iridescent reflection and getting higher aspect ratio has to be maintained. Moreover, surface randomization [28, 41, 42] which also plays a key role in *Morpho* inspired structural colors can be included as well in this design. Combining secondary surface diffuser (aperiodic microstructure by multiwave exposure) [20] with our current technique, almost perfect *Morpho* type 'Christmas tree' structures might be manufactured. Overall, by tuning the exposure wavelength and choosing the photoresist accordingly, structural colors with arbitrary wavelengths can be produced.

Acknowledgments

We acknowledge fruitful discussions with Akira Saito (Osaka University), Guillaume Gomard (KIT), and all members of the Biomimetics group at KIT. This work was partly carried out with the support of the Karlsruhe School of Optics and Photonics (KSOP, www.ksop.ids.kit.edu) and the Karlsruhe Nano Micro Facility (KNMF, www.kit.edu/knmf), a Helmholtz Research Infrastructure at Karlsruhe Institute of Technology (KIT, www.kit.edu). We acknowledge support by Deutsche Forschungsgemeinschaft and Open Access Publishing Fund of Karlsruhe Institute of Technology.